Journal of Computational Chemistry

WILEY

Journal of COMPUTATIONAL CHEMISTRY

RESEARCH ARTICLE OPEN ACCESS

Evaluation of Density-Functional Tight-Binding Methods for Simulation of Protic Molecular Ion Pairs

Tyler Walker[1] | Van-Quan Vuong[2] | Stephan Irle[3] | Jihong Ma[4,5]

[1]Bredesen Center for Interdisciplinary Research and Graduate Education, University of Tennessee, Knoxville, Tennessee, USA | [2]Department of Chemistry, Boston University, Boston, Massachusetts, USA | [3]Computational Sciences and Engineering Division, Oak Ridge National Laboratory, Oak Ridge, Tennessee, USA | [4]Department of Mechanical Engineering, University of Vermont, Burlington, Vermont, USA | [5]Department of Physics, University of Vermont, Burlington, Vermont, USA

Correspondence: Stephan Irle (irles@ornl.gov) | Jihong Ma (jihong.ma@uvm.edu)

Received: 7 September 2024 | **Revised:** 26 November 2024 | **Accepted:** 30 January 2025

Funding: This work was supported by the US Department of Energy, (Grants DE-AC05-00OR22725 and DE-SC0023473), National Science Foundation (Grant 2132055), and the University of Tennessee, Knoxville, Energy Science and Engineering Fellowship.

Keywords: benchmarks | density-functional tight-binding methods | ion pairs | ionization potentials | proton transfer

ABSTRACT

In this work, we benchmark the accuracy of the density-functional tight-binding (DFTB) method, namely the long-range corrected second-order (LC-DFTB2) and third-order (DFTB3) models, for predicting energetics of imidazolium-based ionic liquid (IL) ion pairs. We compare the DFTB models against popular density functionals such as LC-ωPBE and B3LYP, using ab initio domain-based local pair-natural orbital coupled cluster (DLPNO-CC) energies as reference. Calculations were carried out in the gas phase, as well as in aqueous solution using implicit solvent methods. We find that the LC-DFTB2 model shows excellent performance in the gas phase and agrees well with reference energies in implicit solvent, often outperforming DFTB3 predictions for complexation energetics. Our study identifies a range of opportunities for use of the LC-DFTB method and quantifies its sensitivity to protonation states and the types of chemical interactions between ion pairs.

1 | Introduction

Understanding ionic solvent structure through atomistic simulations is a prerequisite for designing ionic solutions in geochemical [1] or chemical energy storage [2] contexts, and advancing a range of technologies, from self-healing ionic polymers for molecular electronics [3] to novel 3D printing approaches [4]. Imidazolium-based organic solvents are of particular interest due to the abundance of imidazolium derivatives in ionic liquid (IL) compounds. Imidazolium derivatives are likewise prevalent in alkaloids [5], biological systems [6], and synthetic pharmaceutical products [7]. Moreover, covalently connected polyamide ionenes (PA-ionenes) containing imidazolium rings were found to exhibit intrinsic, rapid, shape memory, and self-healing behaviors at room temperature [8–10]. Previous work suggested that hydrogen bonds (primarily between the counter-anions and the cationic PA-ionene chains) are responsible for the polymer self-healing process [8]. However, this analysis was based on classical molecular dynamics (CMD) simulations, which are computationally inexpensive yet limited by an empirical treatment of interatomic potentials and charges, and unable to describe proton transfer or other chemical reactions. A more rigorous quantum chemical treatment of these processes is therefore desirable, for instance with density functional theory (DFT); however, calculating the dynamic properties of large-scale polymeric systems using DFT remains challenging due to the high computational cost.

As a middle ground in terms of computational resource requirements, density-functional tight-binding (DFTB) quantum chemical methods offer a compromise by accelerating DFT by two to three orders of magnitude, maintaining comparable

accuracy to DFT, and providing variationally derived electronic structures for every geometry [11]. As an approximation to DFT, DFTB is based on a two-center approximation to the Kohn–Sham Hamiltonian using a minimal basis set for valence-shell electrons and empirically optimized pseudoatomic orbitals [12]. Core electron interactions, nuclear repulsion energies, and double-counting terms are accounted for by way of distance-dependent interatomic repulsion potentials. The Hamiltonian and overlap matrix elements are precalculated within the basis of the pseudoatomic orbitals and tabulated as a function of interatomic distance, permitting a faster time-to-solution with DFTB than with conventional DFT [13]. If applicable to self-healing IL systems, DFTB would offer a good compromise between computational speed and reliable treatment of critical chemical interactions such as proton transfer and polarization effects, while avoiding pitfalls of classical methods, among them empirical interatomic potentials and atomic charges [14–16].

The DFTB models emerge from Taylor expansions of the Kohn–Sham DFT energy around a reference electron density with respect to a density fluctuation, which gives rise to the second-order (DFTB2) and third-order (DFTB3) formalisms [11]. While DFTB2 considers on-site and interatomic charge interactions via Mulliken point charges and a γ-function, which approximates a Coulomb-like interaction of exponentially decaying charge density [11], the DFTB3 formalism further considers the variation of atomic chemical hardness with the corresponding atomic charge state [17].

In previous studies, DFTB3 was reported to be an efficient, accurate method for studying protic IL structures and properties [16, 18]. Addicoat et al. [16] benchmarked DFTB3 against hybrid DFT model chemistry reference energies and concluded that DFTB3 was a suitable choice for predicting complexation energies for molecular clusters containing up to 15 ion pairs. For such molecular clusters, external charge stabilization obscures the role of charge transfer, polarization, and further, the types of chemical interactions occurring between ion pairs. This warrants study of individual ion pairs to more fundamentally understand method performance. Moreover, it is known that self-interaction errors (SIEs) inherited from the semi-local treatment of electronic exchange affect both DFT and DFTB methods [19]. These SIEs may overestimate charge delocalization and underestimate ion pair stabilization [20], making them, particularly, problematic for protic ILs, where either zwitterionic salts or hydrogen-bonded molecular complexes can persist. In ab initio methods such as the gold-standard coupled cluster (CC) method, SIEs are completely absent due to explicit accounting of electrons for electron exchange.

To address SIEs in DFT methods that prioritize low computational resource requirements, an empirical long-range correction (LC) is often employed [21]. By extending a similar correction to the DFTB framework, it was recently shown that long-range corrected second-order DFTB [21, 22] (LC-DFTB2) could effectively overcome many deficiencies of DFTB without LC [21–23], including large SIEs. This is accomplished by incorporating a Hartree–Fock-like exchange to the γ-function at long inter-electron distances, where the local density approximation incorrectly models the exchange interaction [21]. In this paper, we, therefore, focus on the applicability of LC-DFTB2 [24] to IL systems and polymers with charged residues. We place special emphasis on complexation energies (also referred to as ion pair formation energies) essential for qualitatively accurate predictions in IL and ionic polymer simulations featuring large system sizes or time depths. For a quality model, these reaction energies must be in qualitative agreement with predictions from accurate correlated electronic structure methods such as CC.

In this work, we evaluate conventional DFTB3 [17] as well as LC-DFTB2 [24] methods and their predictions of individual ion pair energetics, noting that an LC-DFTB3 method and associated parameters have yet to be developed. We compare DFTB model complexation and isomerization energies against predictions from various DFT and CC methods. The purpose of our work is to give charge- and solvent environment-specific recommendations for IL simulations with quantum chemical methods.

Our work represents a fundamental first step toward simulating large PA-ionene chains and aggregates via DFTB methods, with reliable treatment of ion pair chemistry. Meanwhile, conclusions from this work complement the Addicoat et al. [16] benchmark by selecting systems without external charge stabilization and calculating the complexation, (de)protonation, and salt formation energies of individual IL ion pairs against CC reference energies.

Our work is organized as follows: first, we introduce our selection of IL model systems, including the ionic and neutral complexes employed in the benchmark (Section 2.1). We then validate the domain-based local pair natural orbital [25] (DLPNO) approximation to CC with singles, doubles, and perturbative triples [26] [CCSD(T)] for these systems (Section 2.2.1). Benchmarking results against the DLPNO-CCSD(T) reference energies are then reported for calculations in the gas phase (Section 3.1) and aqueous solution (Section 3.2), for which we apply a solute molecule density continuum solvation model (SMD) [27] and a conductor-like screening model (COSMO) [28]. Including solvated benchmarks was motivated by experimental observation of residual water content [29] during IL polymer synthesis. Our benchmarks focus on the accuracy of relative energies: complexation energies and ion (de)protonation energies in both gas phase and aqueous medium. We discuss the performance trends of the LC-DFTB and DFTB3 models and conclude with comments on their suitability for simulating these systems, suggesting potential future directions for method development.

2 | Methodology

2.1 | Model Systems

Due to the limited set of available chemical elements, H, C, N, O, and S, in the ob2′ ($\omega = 0.3$) parameter set [30] for LC-DFTB2 calculations, we selected the acetate (Ac), mesylate (Mes), and methyl bisulfate (Mbs) anions. As cations, we chose imidazolium (Im), 1-methylimidazolium (MIm), and 1-ethyl-3-methylimidazolium (EMim), shown in Figure 1.

Nine ion pairs were derived from the three cations and three anions, with further speciation into zwitterionic, neutral, and covalent forms for each ion pair. The ionic form had the imidazolium cation and (deprotonated) organic acid anion interacting as a salt, while the neutral form contained the imidazole and

organic acid. The covalent form was inspired by observations of dynamic covalent interactions between conjugated ionic liquids and CO_2 [31]. This form was prepared as a Lewis acid–base adduct, with a C–O covalent bond between the imidazolium cation (Lewis acid) and the deprotonated organic acid anion (Lewis base). The geometries for each cation, anion, and their neutral conjugates were fully optimized prior to their use for constructing the initial coordinates for the 27 total possible ion pair complexes, as described in Section 2.2.2. Since we are also interested in the performance of the methods in aqueous solution, we repeated all geometry optimizations and energy calculations with SMD, which gave rise to a final total of $2 \times 27 = 54$ initial ion pair complex geometries that were then carried forward for further geometry optimization.

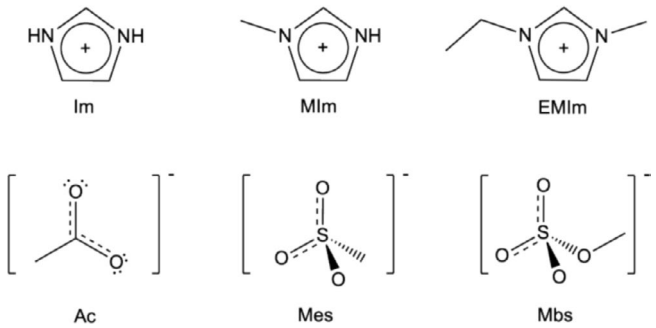

FIGURE 1 | Imidazolium-based cations and the organic anions considered in this work. Nine ion pairs were composed from imidazolium (Im), 1-methyl-imidazolium (MIm), 1-ethyl-3-methyl-imidazolium (EMIm), acetate (Ac), mesylate (Mes), and methyl bisulfate (Mbs).

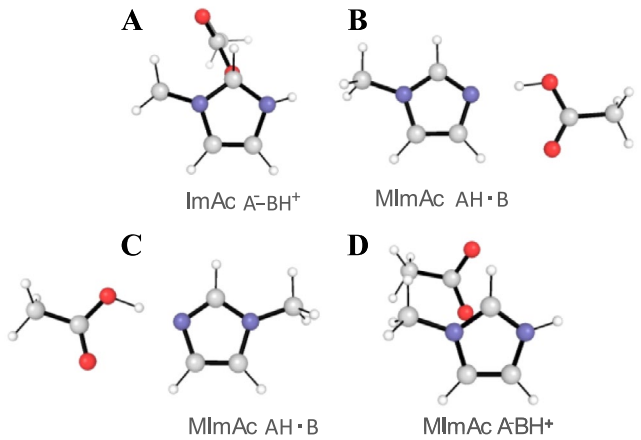

FIGURE 2 | Optimized geometries for methyl-imidazolium acetate complexes. (A) Gas-phase covalent complex, (B) gas-phase neutral complex, (C) solvated neutral complex, and (D) solvated zwitterionic complex.

As anticipated, several structural isomers emerged from this set of 54 geometry optimizations. An example is given in Figure 2 with MImAc complexes in gas phase and solution. Table 1 defines the labeling system used to distinguish complexes obtained after optimization. For convenience, we introduce an acid–base notation to label the complexes assessed by our benchmark, with AH as acid (e.g., acetic acid) and B as base (molecules containing the imidazole unit), $[A]^-$ as conjugate base of the organic acid, and $[BH]^+$ as the imidazolium conjugate acid of the imidazole base. Where multiple initial coordinate conditions relaxed to near structural isomers, the lowest-energy structure was carried forward. This process reduced the initial 54 complex structures to 24 systems, namely 12 gas-phase systems, and 12 solvated systems.

2.2 | Electronic Structure Methods

2.2.1 | CC Methods

CC methods were selected to provide high-accuracy references for the ion pairing energetics. The CC calculations were performed using the ORCA v. 5.0.4 electronic structure program [32, 33], with single and double excitations (CCSD) as well as single, double, and perturbative triple excitations [CCSD (T)]. Dunning's augmented correlation-consistent double-zeta (aug-cc-pVDZ) and triple-zeta (aug-cc-pVTZ) basis sets [34, 35] were used. DLPNO-CC calculations [26, 36] were performed with additional contracted auxiliary basis sets for both aug-cc-pVDZ and aug-cc-pVTZ [37, 38]. The self-consistent field (SCF) energy convergence criterion for the underlying Hartree–Fock calculations was 10^{-8} Hartree (abbreviated as a.u.). The cost-effective DLPNO approximation was compared against full CCSD(T)/aug-cc-pVDZ calculations, including both gas phase and implicit solution. Figure S1 is a parity plot comparing the CCSD(T)/aug-cc-pVDZ and DLPNO-CCSD(T)/aug-cc-pVDZ gas phase complexation energies relative to ionic species at infinite separation. An analogue relative to neutral species at infinite separation is given in Figure S2, and SMD results are in Figures S3 and S4. The DLPNO-CCSD(T) method is in excellent agreement with full CC, with a mean absolute error (MAE) of 0.7 kcal mol^{-1} in gas phase. With SMD, the DLPNO-CCSD(T) MAE is 0.6 kcal mol^{-1}.

TABLE 1 | Notation for optimized complex structures.

Complex	Label	Formation reactions
Neutral complexes	AH • B	$[A]^- + [BH]^+ \rightarrow$ AH • B (proton transfer) AH + B → AH • B (noncovalent interaction)
Neutral covalent complexes (Lewis adduct)	$[A]^-$–$[BH]^+$	$[A]^- + [BH]^+ \rightarrow [A]^-$–$[BH]^+$ (Lewis addition)
Zwitterionic complexes	$[A]^-[BH]^+$	$[A]^- + [BH]^+ \rightarrow [A]^-[BH]^+$ (ion association)

We thus selected the DLPNO-CCSD(T) method as the benchmark reference for all energy comparisons.

2.2.2 | DFT Methods

All DFT calculations were performed using ORCA v. 5.0.4 [32]. We computed reaction energetics using the B3LYP [39, 40] and LC-ωPBE [41, 42] DFT functionals. For the basis set, we selected Pople's 6–311 + G(d, p) [43–47] valence triple zeta fully polarized basis set. As for the CC calculations, the SCF convergence criterion was 10^{-8} a.u. for all calculations.

Geometries for each ion and its conjugate base excepting EMIm, whose neutral conjugate base breaks the ring aromaticity and was not considered in this work, were optimized at the LC-ωPBE/6–311 + G(d, p) level of theory prior to generating initial geometries for complexes. We selected this level of theory because it was found in an earlier study to outperform generalized gradient approximation (GGA) and fixed hybrid DFT methods for the geometries of imidazolium-based ILs [48]. The initial coordinates were prepared in Avogadro v. 1.2.0 [49] by orienting the two species at positions that were chemically reasonable for hydrogen bonding interactions. Three cases were considered for each pair: the anion interacting with the cation, the neutral proton transfer complex, and the covalent Lewis adduct. In several cases, different initial conditions produced different complex geometries, from which we consistently carried forward the lowest-energy structure. After generating initial geometries for the pair complexes following the classifications listed in Table 1, fully optimized LC-ωPBE/6–311 + G(d, p)-level geometries were obtained for each complex. For SMD calculations geometries for the ions, neutral conjugates, and complexes were obtained at the LC-ωPBE/6–311 + G(d, p)/SMD level of theory. A dielectric constant of 78.4 was selected to represent water at room temperature.

2.2.3 | DFTB Methods

DFTB calculations were carried out with the DFTB+ v. 21.1 [50] program using Grimme dispersion (D3) [51] with two sets of optimized dispersion constants, one reported by Gaus et al. [52] and the other by Brandenburg and Grimme [53], along with Becke–Johnson (BJ) damping [54] corrections with the respective LC-DFTB2-D3(BJ)/ob2′ ($\omega = 0.3$) [30] and DFTB3-D3(BJ)/3ob [55] models and levels of theory. We leave calculations with the Brandenburg dispersion constants to the supplement, as Gaus' dispersion model is a common default implementation (as in DFTB+). The self-consistent charge (SCC) convergence criterion was 10^{-8} a.u., the same threshold as the SCF convergence criterion for the CC and DFT calculations.

Since the SMD model is not yet implemented in DFTB+, we instead tested two available implicit solvent methods, the COSMO [28] and Generalized Born [56] with solvent-accessible surface area (GBSA) methods. The GBSA model used parameters from Ehlert et al. [57] (see Tables S11–S14 for comparison). For COSMO, a range of rescaling for the van der Waals radii were compared against the reference energies, and the best-performing model, a 1.5× radius rescaling, was carried forward.

2.3 | Geometry Optimizations

Molecular structures for all benchmarked systems were fully optimized at the LC-ωPBE-D3(BJ)/6–311 + G(d,p) level of theory, both in gas phase and in SMD aqueous solution. For all other methods, single-point energies were computed using the corresponding LC-ωPBE-D3(BJ)/6–311 + G(d,p)-optimized geometries, except for the water molecule [58] and the hydronium ion [59], for which structures were taken from the corresponding references. During the LC-ωPBE-D3(BJ)/6–311 + G(d,p) geometry optimization cycles, some ion pairs relaxed to zwitterionic, neutral, or covalent forms irrespective of the protonation state of the initial complex coordinates. In these cases, the lowest-energy structure was carried forward as the representative structure for the respective system.

2.4 | Relative Energy Quantities

We are computing the following relative energy quantities: protonation energies for the bases and deprotonation energies for the acids, complexation energies with respect to both neutral and ionic individual components, and salt formation energies. Table 2 collects the chemical reactions we assessed. In Table 2, the symbol "•" indicates a hydrogen-bonded complex, while the symbol "–" indicates a covalent bond between the two components in a Lewis adduct.

The relative energies, ΔE, are defined following the convention $\Delta E = E_{\text{products}} — E_{\text{reactants}}$ for all chemical reactions listed above, with reactants at left of the reaction arrow. In this convention, a negative value of ΔE indicates an exothermic process, whereas a positive ΔE indicates an endothermic process.

TABLE 2 | Chemical reactions and definitions for relative energy benchmarks.

Reaction type	Example
Acid deprotonation	$AH + H_2O \rightarrow [A]^- + [H_3O]^+$
Conjugate acid deprotonation (imidazolium cations)	$[BH]^+ + H_2O \rightarrow B + [H_3O]^+$
Complexation (zwitterions)	$[A]^- + [BH]^+ \rightarrow [A]^-[BH]^+$
Proton transfer	$[A]^- + [BH]^+ \rightarrow AH \bullet B$
Salt formation energy	$AH + B \rightarrow [A]^-[BH]^+$
Lewis addition (covalent complexes)	$[A]^- + [BH]^+ \rightarrow [A]^- - [BH]^+$

We compute the MAEs and mean absolute deviations of the errors (MAD) to assess the relative energy quantities, using their standard definitions. These summary statistics are compared in Formulas (1) and (2), where y_i are the reaction energies for each method, x_i are the reference energies, and $M(y)$ is the signed mean of the reaction energy errors from y_1 to y_i:

$$\mathrm{MAE} = \frac{\sum_{n=1}^{i} |y_i - x_i|}{n} \quad (1)$$

$$\mathrm{MAD} = \frac{\sum_{n=1}^{i} |y_i - M(y)|}{n} \quad (2)$$

While the MAE describes the errors for reaction energies observed for each method (relative to the reference DLPNO-CCSD(T) calculations) the MAD of errors describes the dispersion of those errors, as an indicator for whether the magnitude of the errors is consistent across ion pairs and types of complexes. For concision in presenting the results, "MAD of errors" is abbreviated to MAD in the following sections.

3 | Results and Discussion

In the following subsections, we present benchmark comparisons for complexation energies, acid deprotonation energies, as well as salt formation energies, as defined in Table 2. We report gas-phase benchmarks before discussing SMD and COSMO implicit solvent results.

3.1 | Gas-Phase Calculations

We note that the EMIm cation cannot be deprotonated to a neutral conjugate base and is, therefore, treated only as a cation in our calculations.

3.1.1 | Complexation Energies for Neutral Complexes

Complexation energies for neutral complexes are shown in Figure 3, with respect to ions in Figure 3A and with respect to neutral species in Figure 3B.

In Figure 3A, LC-DFTB2 shows an MAE of 6.0 kcal mol^{-1} and MAD 4.6 kcal mol^{-1}. DFTB3 has the lowest performance of the assessed methods, with MAE 11.7 kcal mol^{-1} and MAD 2.3 kcal mol^{-1}. LC-ωPBE is comparable to LC-DFTB with MAE 6.0 kcal mol^{-1} and MAD 2.7 kcal mol^{-1}. Notably, B3LYP has the lowest errors and lowest deviation of errors, with MAE 3.2 kcal mol^{-1} and MAD 2.1 kcal mol^{-1}.

The complexation energies for neutral complexes from neutral species in Figure 3B follow a similar trend for method performance. LC-DFTB2 shows MAE 3.9 kcal mol^{-1} and a high deviation of errors, with MAD 4.4 kcal mol^{-1}. DFTB3 has higher errors than LC-DFTB2 with MAE 6.0 kcal mol^{-1} and MAD 2.2 kcal mol^{-1}. LC-ωPBE has MAE 7.6 kcal mol^{-1} and MAD 2.5 kcal mol^{-1}. B3LYP again has the best performance with MAE 1.7 kcal mol^{-1} and MAD 1.6 kcal mol^{-1}. Ranking the method performance for complexation energies of neutral complexes in the gas phase, we find B3LYP>LC-ωPBE ~ LC-DFTB2 > DFTB3.

3.1.2 | Relative Protonation and Deprotonation Energies

Figure 4 shows relative deprotonation energies for imidazolium acids in Figure 4A and the organic anion acids in Figure 4B. In both sets of systems, LC-DFTB2 significantly underperforms DFTB3 with an MAE of 11.2 kcal mol^{-1}, where DFTB3 shows MAE 3.9 kcal mol^{-1}, comparable to LC-ωPBE with MAE 2.3 kcal mol^{-1}. B3LYP again has the best performance with MAE 1.4 kcal mol^{-1}. For the DFT methods, the deprotonation

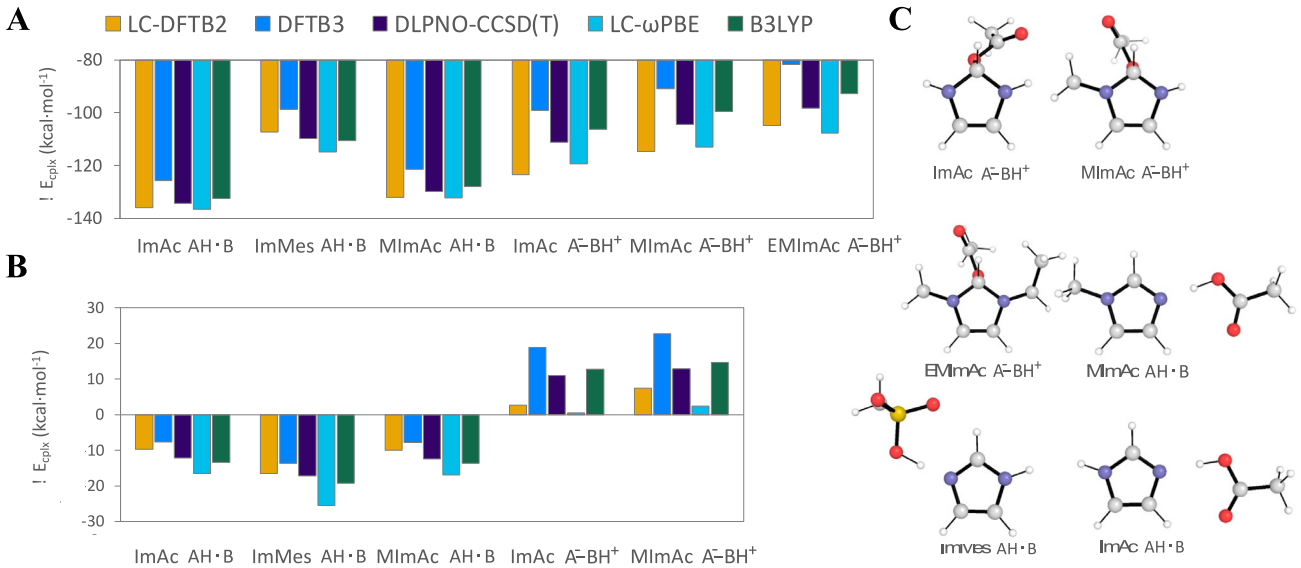

FIGURE 3 | Complexation energies in kcal mol^{-1} for neutral complexes with respect to ions (A) and to neutral species (B). Geometries of the neutral complexes (C).

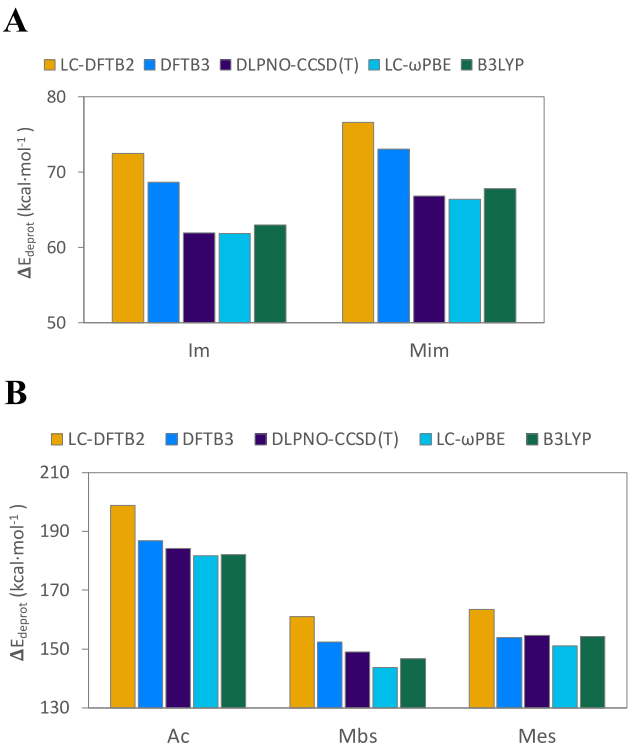

FIGURE 4 | Relative deprotonation energies for imidazole conjugate acids (A) and organic acids in kcal mol^{-1} (B). Water was added across the reactions, giving $[BH]^+ + H_2O \rightarrow B + [H_3O]^+$.

of the Mbs acid shows the highest error, at 5.4 kcal mol^{-1} for LC-ωPBE and 2.4 kcal mol^{-1} for B3LYP. Regarding DFTB methods, we do not find a clear trend in errors, with LC-DFTB2 having high errors for both imidazolium species, MAE 10.2 kcal mol^{-1}, and anion acids, MAE 11.9 kcal mol^{-1}. DFTB3 has MAE 6.5 kcal mol^{-1} for imidazolium species, but low errors for anion acids, MAE 2.2 kcal mol^{-1}.

3.1.3 | Complexation Energies for Ionic Complexes

Complexation energies for zwitterions are shown in Figures 5 and 6. Energies in Figure 5 are relative to ions at infinite separation. LC-DFTB2 shows low errors with MAE and MAD 0.9 kcal mol^{-1}. The contribution of Grimme's dispersion model [53] is small, having the same magnitude of errors at 0.9 kcal mol^{-1} and slightly lower error deviation with MAD 0.7 kcal mol^{-1}. Meanwhile, DFTB3 shows higher errors and deviations with MAE 5.2 kcal mol^{-1} and MAD 3.5 kcal mol^{-1}. LC-ωPBE has similar errors with MAE 5.4 kcal mol^{-1} and MAD 0.7 kcal mol^{-1}. B3LYP again performs best, with MAE and MAD of 0.5 kcal mol^{-1}. For complexation energies of zwitterions with respect to ions, we thus find that the performance follows B3LYP>LC-DFTB2 > DFTB3 ~ LC-ωPBE.

Figure 6 displays the complexation energies relative to neutral species at infinite separation. LC-DFTB2 has low errors, with MAE 0.9 kcal mol^{-1} and MAD 0.7 kcal mol^{-1}. DFTB3 shows MAE

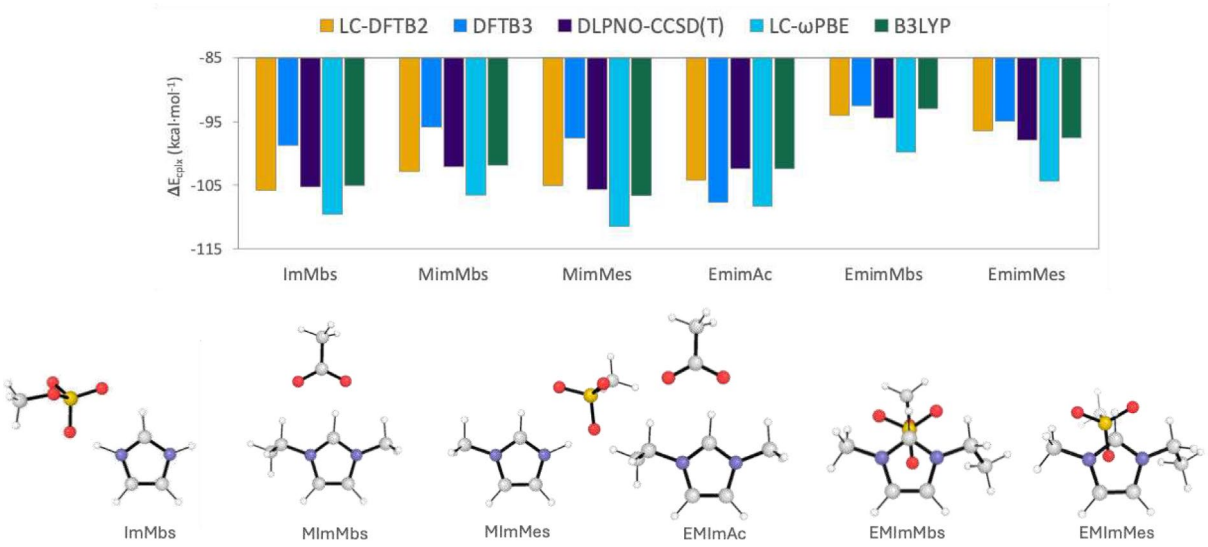

FIGURE 5 | Complexation energies for zwitterionic complexes with respect to ions in kcal mol^{-1}.

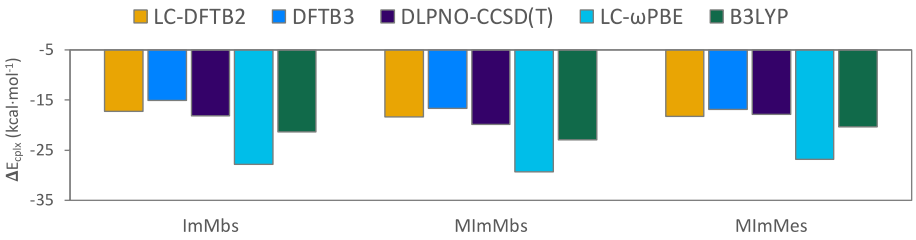

FIGURE 6 | Complexation energies for zwitterionic complexes with respect to neutral species in kcal mol^{-1}.

2.4 kcal mol^{-1} and MAD 0.9 kcal mol^{-1}. LC-ωPBE has the highest error with MAE 9.4 kcal mol^{-1} and MAD 0.3 kcal mol^{-1} and B3LYP has MAE 2.9 kcal mol^{-1} and MAD 0.3 kcal mol^{-1}. For complexation energies of zwitterions with respect to neutral species, we thus rank the performances as LC-DFTB2 > DFTB3 ~ B3LYP>LC-ωPBE.

Across all the assessed complexation reactions, presented in Figures 3–6, LC-DFTB2 has an MAE of 3.1 kcal mol^{-1} and an MAD of 2.8 kcal mol^{-1}, Meanwhile, DFTB3 performs similarly to LC-ωPBE, with MAE 6.9 kcal mol^{-1} and MAD 2.5 kcal mol^{-1}. LC-ωPBE shows MAE 6.7 kcal mol^{-1} and MAD 1.7 kcal mol^{-1}, whereas B3LYP performs best among the assessed methods across these complexation reactions, with MAE 2.0 kcal mol^{-1} and MAD 1.2 kcal mol^{-1}. In the gas phase, we summarize the method performance ranking as B3LYP>LC-DFTB2 > LC-ωPBE ~ DFTB3.

3.2 | Implicit Solvent Calculations

3.2.1 | Complexation Energies for Neutral Complexes in Aqueous Solution

Figure 7 shows the complexation energies for neutral complexes with respect to ions in Figure 7A and to neutral species in Figure 7B, each in implicit solvent using aqueous medium. For the complexation of neutral complexes with respect to ionic species in Figure 7A, both DFTB flavors have the highest errors. LC-DFTB2 shows MAE 8.4 kcal mol^{-1} and MAD 3.1 kcal mol^{-1} and exhibits a large maximum error of 14.7 kcal mol^{-1} for covalent EMImAc. DFTB3 has MAE 7.8 kcal mol^{-1} and MAD 5.9 kcal mol^{-1}. DFTB3 has high errors for neutral covalent complexes as well, ranging from 10.7 to 16.8 kcal mol^{-1}, but lower errors for proton transfer (AH • B) complexes, with errors of 2.1 kcal mol^{-1} for ImAc and 1.6 kcal mol^{-1} for MImAc. Both DFT methods have low errors and low deviation in their errors. LC-ωPBE shows MAE 4.0 kcal mol^{-1} and MAD 2.2 kcal mol^{-1}, and B3LYP performs the best with MAE 3.5 kcal mol^{-1} and MAD 2.4 kcal mol^{-1}. For these reactions in aqueous solution, we find that the performance ranking is B3LYP ~ LC-ωPBE>DFTB3 > LC-DFTB2.

For the complexation energies of neutral complexes with respect to neutral species in Figure 7B, LC-DFTB2 shows MAE 2.4 kcal mol^{-1} and MAD 2.3 kcal mol^{-1}, while DFTB3 has MAE 2.9 kcal mol^{-1} and MAD 3.8 kcal mol^{-1}. In this subset of the complexation energies, LC-DFTB2 follows the performance trend of DFTB3, with errors less than 1 kcal mol^{-1} for the AH • B complexes (ImAc and MImAc), but a higher error for covalent ImAc $[A]^- - [BH]^+$ at 5.9 kcal mol^{-1}. LC-ωPBE has the highest errors overall with MAE 6.1 kcal mol^{-1} and MAD 1.8 kcal mol^{-1}. B3LYP again shows the lowest errors with MAE 1.9 kcal mol^{-1} and MAD 1.9 kcal mol^{-1}. For these reactions, B3LYP>DFTB2 ~ DFTB3 > LC-ωPBE.

3.2.2 | Relative Protonation and Deprotonation Energies

Figure 8 shows the relative deprotonation energies of imidazolium acids in Figure 8A and the organic anion acids in Figure 8B. Both DFTB methods show high errors for deprotonation reactions in implicit solvent. LC-DFTB2 has MAE 12.8 kcal mol^{-1}, whereas DFTB3 has high MAE 17.0 kcal mol^{-1}. Both LC-DFTB2 and

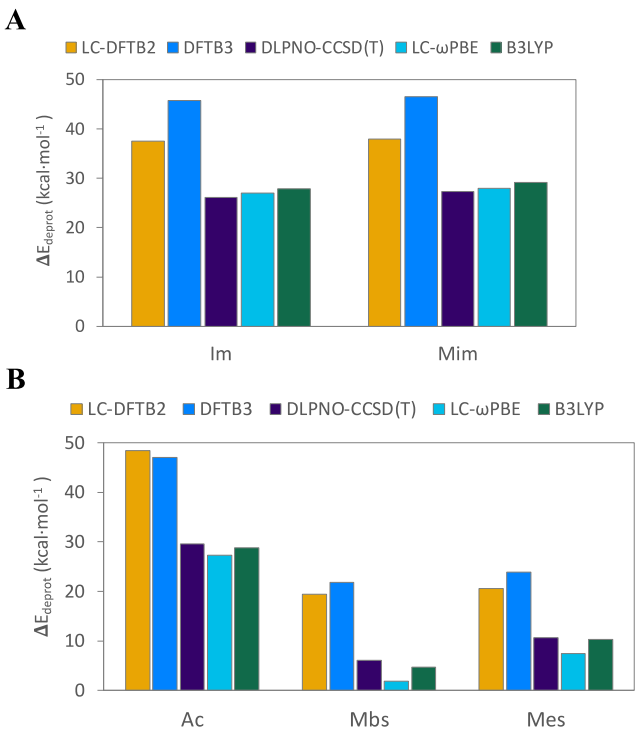

FIGURE 7 | Complexation energies for neutral complexes with respect to ions (A) and neutral species (B) in implicit solvent (kcal mol^{-1}). Geometries for the solvated neutral complexes are shown in (C).

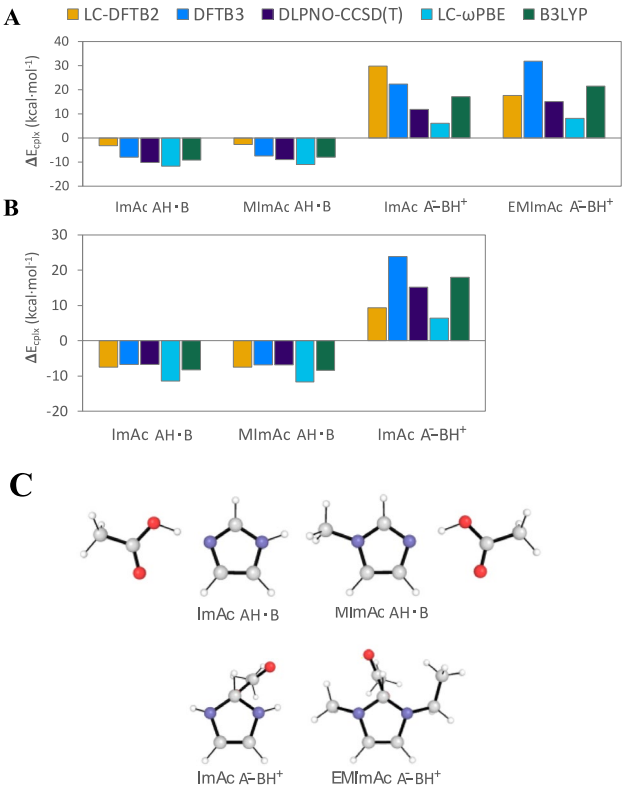

FIGURE 8 | Relative deprotonation energies for conjugate acids of the (A) cations and (B) anions in kcal mol^{-1}. Water was added across the reactions, giving $[BH]^+ + H_2O \rightarrow B + [H_3O]^+$.

DFTB3 show, particularly, high errors for the deprotonation of acetic acid, with 18.8 kcal mol^{-1} for LC-DFTB2 and 17.5 kcal mol^{-1} for DFTB3. Meanwhile, the DFT methods show low errors, with LC-ωPBE MAE of 2.2 kcal mol^{-1} and B3LYP MAE of 1.2 kcal mol^{-1} across all deprotonation reactions. Consistent with the gas phase trend, LC-DFTB2 better reproduces the imidazolium acid deprotonations, with MAE 11.0 kcal mol^{-1}, than the organic anion acid deprotonations, MAE 14.0 kcal mol^{-1}. DFTB3 has higher errors in both cases, with MAE 19.4 kcal mol^{-1} for imidazolium species and MAE 15.5 kcal mol^{-1} for organic anion acids. LC-ωPBE again shows its highest error for deprotonation of Mbs at 4.2 kcal mol^{-1}. B3LYP has low errors across deprotonation reactions, with all errors below 2.0 kcal mol^{-1}. Here, the order for method performance is B3LYP > LC-ωPBE > LC-DFTB2 > DFTB3.

3.2.3 | Complexation Energies for Ionic Complexes

Complexation energies for zwitterionic complexes are shown in Figure 9, with respect to ions in Figure 9A, and with respect to neutral species in Figure 9B. Figure 9C includes structures of all ionic complexes optimized in an implicit water solvent. Starting with complexation energies for zwitterionic complexes with respect to ions in Figure 9A, the errors are low with MAE fewer than 3 kcal mol^{-1} for all assessed methods. LC-DFTB2 and DFTB3 perform similarly, each with MAE and MAD of 0.7 kcal mol^{-1}. DFTB3 shows a maximum error of 1.3 kcal mol^{-1} for MImAc, lower than the LC-DFTB2 error of 1.6 kcal mol^{-1}. LC-ωPBE shows MAE 1.6 kcal mol^{-1} and MAD 0.4 kcal mol^{-1}, whereas again B3LYP has the best performance with MAE and MAD of 0.6 kcal mol^{-1}. Here, B3LYP > DFTB3 ~ LC-DFTB2 > LC-ωPBE.

Moving to complexation energies for zwitterionic complexes with respect to neutral species, shown in Figure 9B, LC-DFTB2 shows low errors with MAE 4.6 kcal mol^{-1} and MAD 4.1 kcal mol^{-1}. LC-DFTB2 has a high error for MImAc, at 9.4 kcal mol^{-1}. Meanwhile, DFTB3 has MAE 3.8 kcal mol^{-1} and MAD 1.9 kcal mol^{-1}, and instead shows the highest errors for sulfur-containing complexes. All errors for DFTB3 are less than 6.4 kcal mol^{-1}. LC-ωPBE shows MAE 5.7 kcal mol^{-1} and MAD 0.8 kcal mol^{-1}, and B3LYP again has the best performance with

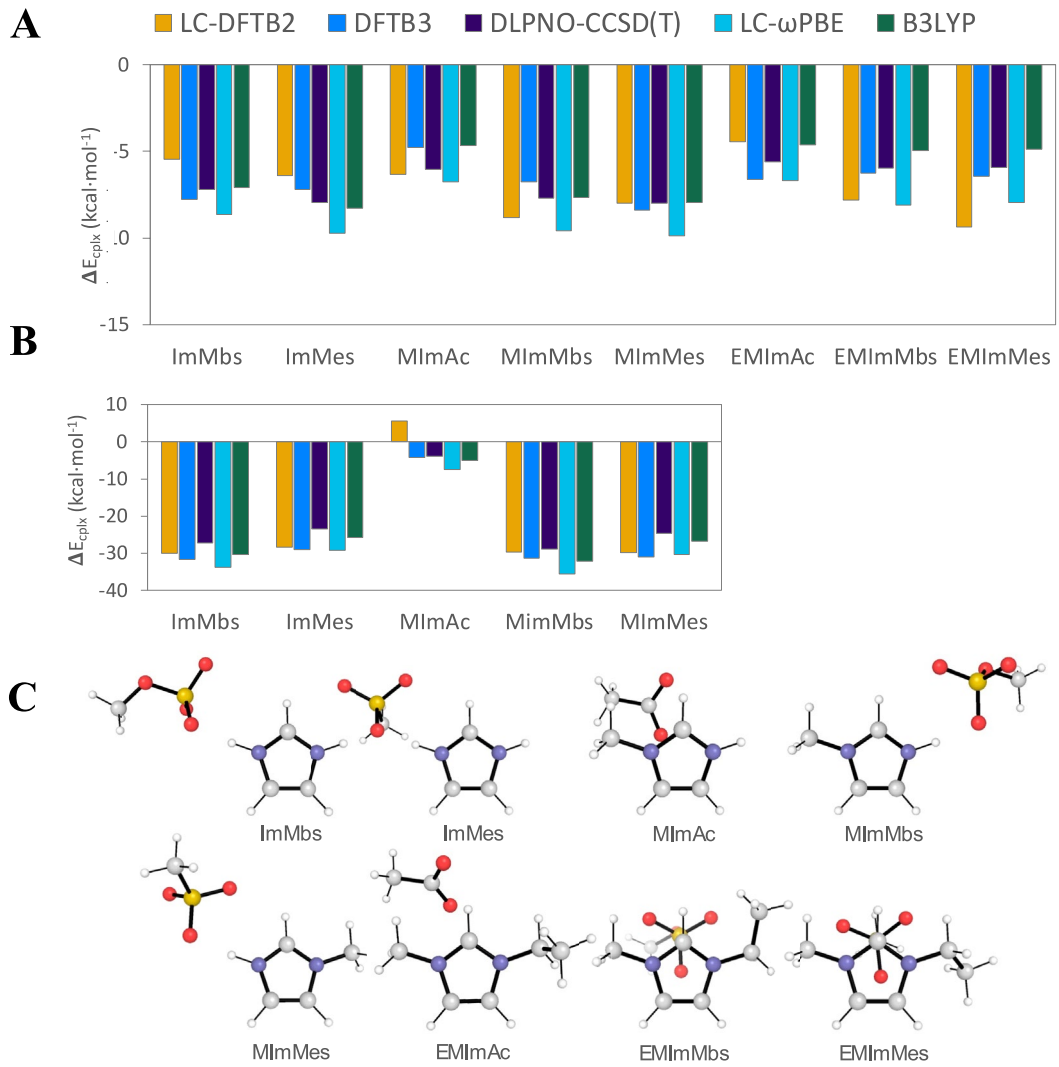

FIGURE 9 | Complexation energies for solvated zwitterionic complexes with respect to ions (A) and to neutral complexes (B) in kcal mol^{-1}. Geometries for solvated zwitterionic complexes are shown in (C).

MAE 2.4 kcal mol^{-1} and MAD 0.6 kcal mol^{-1}. For these reactions, B3LYP>DFTB3 ~ LC-DFTB2 > LC-ωPBE.

Across all complexation reactions in implicit solvent (shown in Figures 7–9), LC-DFTB2 shows MAE 3.5 kcal mol^{-1} and MAD 2.3 kcal mol^{-1}. Meanwhile, DFTB3 exhibits low errors, consistent with the earlier results by Addicoat et al. [16], with MAE 3.2 kcal mol^{-1} and MAD 2.5 kcal mol^{-1}. LC-ωPBE also shows low errors with MAE 3.8 kcal mol^{-1} and MAD 1.1 kcal mol^{-1}. B3LYP again outperforms all other assessed methods with MAE 1.8 kcal mol^{-1} and MAD 1.1 kcal mol^{-1}. Across all reactions in implicit solvent, B3LYP>DFTB3 ~ LC-DFTB2 ~ LC-ωPBE.

As we can see from the above comparisons, while DFTB3 and LC-DFTB2 have a similarly strong performance in implicit aqueous solution, with an overall total MAE of 3.2 kcal mol^{-1} for DFTB3 and MAE 3.5 kcal mol^{-1} for LC-DFTB2, LC-DFTB2 performs better than DFTB3 in the gas phase, with MAE 3.1 kcal mol^{-1} where DFTB3 has an MAE 6.9 kcal mol^{-1}. Table 3 summarizes the gas phase results and Table 4 summarizes the implicit aqueous solvation results. Analogous tables with MAD are included in Tables S6 and S18.

To understand the excellent LC-DFTB2 performance in the gas phase and inform possible routes for future method development or parameterization work, additional tests were performed to assess factors contributing to the observed performance which will be briefly summarized here (see Supporting Information for details, including Tables S8–S11). As potential factors of influence, we considered the range separation parameter, ω, regulating the LC Hartree–Fock-like exchange contributions to the complexation energetics, and the extent of charge transfer as indicated by the Mulliken charges employed by all DFTB flavors. All tests were performed in the gas phase to avoid external charge delocalization and stabilization effects from the implicit solvent model.

Our analysis suggests that complexation energetics are indeed sensitive to the choice of the range separation parameter and the associated, respectively optimized, repulsion potentials; but mostly insensitive to the magnitude of the charge transfer. We find that the influence of ω on complexation energetics is rather small, on the order of 0.2 kcal mol^{-1} in terms of the MAE, and is insufficient to explain the excellent LC-DFTB2 performance in the gas phase. Meanwhile, we find large differences between the LC-DFTB2 and DFTB3 contributions from the repulsion energy, of several kcal mol^{-1} on average. Surprisingly, we find that the differences between methods are most pronounced for covalent complexes, at 10.8 kcal mol^{-1} with respect to ions and a standout 21.0 kcal mol^{-1} with respect to neutral species. From this analysis, we find that the individually optimized repulsion potentials for each range-separation parameter ω play a central role in the differences in predicted complexation energies between the two methods.

The second-order component of the LC correction appears to distinguish neutral Lewis adducts from neutral proton-transfer complexes, enabling satisfactory and even excellent descriptions of a range of complexes' charge states, from zwitterions to neutral and covalent complexes. When the second-order Fock contribution is neglected, the errors for neutral and covalent complexation energies increase with LC-DFTB2/ob2′ ($\omega = 0.3$), whereas zwitterions are described well with or without that component of the LC. This reflects the anticipated behavior, that the modified treatment of exchange influences bonding interactions but minimally affects nonbonding interactions.

Comparing the DFTB methods with B3LYP/6–311 + G(d,p), the best-performing DFT method, there is up to a four-time increase in Mulliken charge on the ions for covalent complexes. This effect is exacerbated by the minimal pseudoatomic basis sets employed in DFTB, as Mulliken charges are known to be sensitive to the basis set [60]. Despite this response in charge transfer, the

TABLE 3 | Summary of gas-phase method performance by MAE, kcal mol^{-1}.

Reaction	LC-DFTB2	DFTB3	LC-ωPBE	B3LYP
Acid deprotonation	11.2	3.9	2.3	1.4
Complexation, neutral complexes				
With respect to ions	6.0	11.7	6.0	3.2
With respect to neutral species	3.9	6.0	7.6	1.7
Complexation, zwitterions				
With respect to ions	0.9	5.2	5.4	0.5
With respect to neutral species	0.9	2.4	9.4	2.9
All reactions	3.1	6.9	6.7	2.0

TABLE 4 | Summary of implicit solvent method performance by MAE, kcal mol^{-1}.

Reaction	LC-DFTB2	DFTB3	LC-ωPBE	B3LYP
Acid deprotonation	12.8	17.0	2.2	1.2
Complexation, neutral complexes				
With respect to ions	8.4	7.8	4.0	3.5
With respect to neutral species	2.4	2.9	6.1	1.9
Complexation, zwitterions				
With respect to ions	0.7	0.7	1.6	0.6
With respect to neutral species	4.6	3.8	5.7	2.4
All reactions	3.5	3.2	3.8	1.8

differences in complexation energies are on the order of only a few kcal mol^{-1}, insufficient to explain the observed order-of-magnitude higher errors in complexation energies. While differences in the extent of charge transfer between DFTB3 and LC-DFTB2 are often small, the per-atom polarizations show significant differences between these methods. The differences in polarization across methods are of a greater magnitude than the extent of charge transfer estimated with Mulliken charges, reflecting that the signed differences in polarization cancel much of the increased charge when entire molecules rather than individual atoms are considered.

4 | Conclusions

In this work, we investigated ion pairs formed from three commonly used organic acid anions (Ac, Mes, and Mbs) and imidazolium cations (imidazolium, 1-methyl-imidazolium, and 1-ethyl-3-methyl-imidazolium). Complexation and deprotonation energetics were computed using the DLPNO-CCSD(T) method, which we validated against corresponding full CC methods. Our focus was on the benchmark of LC-DFTB2 and DFTB3 as computationally economical approximations to conventional DFT methods.

We paid particular attention to individual ion pairs when assessing errors for the energetics, separating methodological strengths and weaknesses from the compensatory external Coulombic charge stabilizations usually encountered in calculations on larger ion pair clusters. Departing from Addicoat et al. [16], which benchmarked ion pair clusters rather than individual ion pairs, we found that the LC treatment in LC-DFTB2 lends considerable benefit to the gas-phase energetics, with MAE 3.1 kcal mol^{-1}, while the DFTB3 performance declines to MAE 6.9 kcal mol^{-1}. Meanwhile, both DFTB3 and LC-DFTB2 have similarly strong performance with implicit solvent, with a grand total MAE of 3.2 kcal· mol^{-1} for DFTB3 and 3.5 kcal mol^{-1} for LC-DFTB2.

Additionally, the second-order Fock-like component of the LC correction appears to distinguish neutral covalent complexes (Lewis adducts) from proton transfer complexes, enhancing the description of neutral complexes. In the context of IL ion pairs, LC-DFTB2/ob2′ ($\omega = 0.3$) achieves a lower grand total MAE in predicting all reaction energies, with performance exceeding DFTB3/3ob. Such an excellent performance in the gas phase is insufficiently explained by differences in charge transfer. The choice of range separation has a modest impact, while the associated repulsion potentials—individually optimized for the different values of ω—show a significant contribution, with indications for additional flexibility in distinguishing types of neutral complexes by the LC.

Noting conditions where DFTB3 performs well while LC-DFTB2 shows large errors, such as complexation energies for zwitterionic complexes with respect to ions in implicit solvent (Figure 9A), we expect that a future LC-DFTB3 method would bridge the gap in performance and enhance DFTB description of IL ion pairs. Our results indicate that the excellent performance of the DFTB3 method for IL clusters, as reported by Addicoat et al. [16] was fortuitous since charge screening canceled methodological errors of the DFTB method. In such cases, DFTB3 provides excellent energy predictions but insufficiently captures charge transfer and other key physics at the level of ion pairs.

We are hopeful that the conclusions from this comparative study are informative for future large-scale yet accurate simulations of ILs and IL polymers containing the functional groups that we investigated here, as they constitute a broad range of natural products and synthetic derivatives with crucial and advanced functionalities, among them self-healing and shape-memory imidazole-ring-containing PA-ionenes.

Acknowledgments

T.W. acknowledges the support of an Energy Science and Engineering Fellowship from the Bredesen Center for Interdisciplinary Research and Graduate Education at the University of Tennessee, Knoxville. J.M. acknowledges the support of the National Science Foundation (NSF 2132055) and the U.S. Department of Energy (DE-SC0023473). The calculations in this work were in part supported by the Office of Materials and Chemical Technologies within the Office of Nuclear Energy, US Department of Energy. This research used resources of the Compute and Data Environment for Science (CADES) at the Oak Ridge National Laboratory, which is supported by the Office of Science of the US Department of Energy under (DE-AC05-00OR22725).

Data Availability Statement

The data that supports the findings of this study are available in the Supporting Information of this article.

References

1. G. Arrachart, J. Couturier, S. Dourdain, C. Levard, and S. Pellet-Rostaing, "Recovery of Rare Earth Elements (REEs) Using Ionic Solvents," *Processes* 9, no. 7 (2021): 1202.

2. S. Mubarak, D. Dhamodharan, P. N. P. Ghoderao, and H.-S. Byun, "A Systematic Review on Recent Advances of Metal–Organic Frameworks-Based Nanomaterials for Electrochemical Energy Storage and Conversion," *Coordination Chemistry Reviews* 471 (2022): 214741.

3. F. Wang, P. Zhang, G. Wang, A. S. Nia, M. Yu, and X. Feng, "Functional Electrolytes: Game Changers for Smart Electrochemical Energy Storage Devices," *Small Science* 2, no. 2 (2022): 2100080, https://doi.org/10.1002/smsc.202100080.

4. S. Miralles-Comins, M. Zanatta, and V. Sans, "Advanced Formulations Based on Poly(Ionic Liquid) Materials for Additive Manufacturing," *Polymers* 14, no. 23 (2022): 5121, https://doi.org/10.3390/polym14235121.

5. B. Cui, B. L. Zheng, K. He, and Q. Y. Zheng, "Imidazole Alkaloids From Lepidiummeyenii," *Journal of Natural Products* 66, no. 8 (2003): 1101–1103.

6. B. Dolensky and K. L. Kirk, "New Building Blocks for Fluorinated Imidazole Derivatives: Preparation of β-Fluoro- and β,β-Difluorohistamine," *Journal of Organic Chemistry* 66, no. 13 (2001): 4687–4691.

7. X. Zheng, Z. Ma, and D. Zhang, "Synthesis of Imidazole-Based Medicinal Molecules Utilizing the Van Leusen Imidazole Synthesis," *Pharmaceuticals* 13, no. 3 (2020): 37.

8. K. O'Harra, N. Sadaba, M. Irigoyen, et al., "Nearly Perfect 3D Structures Obtained by Assembly of Printed Parts of Polyamide Ionene Self-Healing Elastomer," *ACS Applied Polymer Materials* 2, no. 11 (2020): 4352–4359, https://doi.org/10.1021/acsapm.0c00799.

9. J. Demarteau, K. E. O'Harra, J. E. Bara, and H. Sardon, "Valorization of Plastic Wastes for the Synthesis of Imidazolium-Based Self-Supported Elastomeric Ionenes," *ChemSusChem* 13, no. 12 (2020): 3122–3126.

10. I. Kammakakam, K. E. O'Harra, G. P. Dennis, E. M. Jackson, and J. E. Bara, "Self-Healing Imidazolium-Based Ionene-Polyamide Membranes: An Experimental Study on Physical and Gas Transport Properties," *Polymer International* 68, no. 6 (2019): 1123–1129.

11. M. Elstner and G. Seifert, "Density Functional Tight Binding," *Philosophical Transactions of the Royal Society A: Mathematical, Physical and Engineering Sciences* 372, no. 2011 (2014): 20120483, https://doi.org/10.1098/rsta.2012.0483.

12. G. Seifert and J.-O. Joswig, "Density-Functional Tight Binding—An Approximate Density-Functional Theory Method," *WIREs Computational Molecular Science* 2, no. 3 (2012): 456–465.

13. A. J. Page, A. Elbourne, R. Stefanovic, et al., "3-Dimensional Atomic Scale Structure of the Ionic Liquid–Graphite Interface Elucidated by AM-AFM and Quantum Chemical Simulations," *Nanoscale* 6, no. 14 (2014): 8100–8106.

14. K. Cui, A. Yethiraj, and J. R. Schmidt, "Influence of Charge Scaling on the Solvation Properties of Ionic Liquid Solutions," *Journal of Physical Chemistry B* 123, no. 43 (2019): 9222–9229.

15. G. D. Barbosa, X. Liu, K. E. O'Harra, J. E. Bara, and C. H. Turner, "Charge Scaling Parameter Evaluation for Multivalent Ionic Liquids With Fixed Point Charge Force Fields," *Journal of Ionic Liquids* 2, no. 1 (2022): 100020.

16. M. A. Addicoat, R. Stefanovic, G. B. Webber, R. Atkin, and A. J. Page, "Assessment of the Density Functional Tight Binding Method for Protic Ionic Liquids," *Journal of Chemical Theory and Computation* 10, no. 10 (2014): 4633–4643.

17. M. Gaus, Q. Cui, and M. Elstner, "DFTB3: Extension of the Self-Consistent-Charge Density-Functional Tight-Binding Method (SCC-DFTB)," *Journal of Chemical Theory and Computation* 7, no. 4 (2011): 931–948.

18. A. S. Christensen, J. C. Kromann, J. H. Jensen, and Q. Cui, "Intermolecular Interactions in the Condensed Phase: Evaluation of Semi-Empirical Quantum Mechanical Methods," *Journal of Chemical Physics* 147, no. 16 (2017): 161704, https://doi.org/10.1063/1.4985605.

19. P. Mori-Sánchez, A. J. Cohen, and W. Yang, "Many-Electron Self-Interaction Error in Approximate Density Functionals," *Journal of Chemical Physics* 125, no. 20 (2006): 201102, https://doi.org/10.1063/1.2403848.

20. J. L. Bao, L. Gagliardi, and D. G. Truhlar, "Self-Interaction Error in Density Functional Theory: An Appraisal," *Journal of Physical Chemistry Letters* 9, no. 9 (2018): 2353–2358.

21. T. A. Niehaus and F. Della Sala, "Range Separated Functionals in the Density Functional Based Tight-Binding Method: Formalism," *Physica Status Solidi B* 249, no. 2 (2012): 237–244, https://doi.org/10.1002/pssb.201100694.

22. V. Lutsker, B. Aradi, and T. A. Niehaus, "Implementation and Benchmark of a Long-Range Corrected Functional in the Density Functional Based Tight-Binding Method," *Journal of Chemical Physics* 143, no. 18 (2015): 184107, https://doi.org/10.1063/1.4935095.

23. F. Spiegelman, N. Tarrat, J. Cuny, et al., "Density-Functional Tight-Binding: Basic Concepts and Applications to Molecules and Clusters," *Advances in Physics: X* 5, no. 1 (2020): 1710252.

24. V. Q. Vuong, Y. Nishimoto, D. G. Fedorov, B. G. Sumpter, T. A. Niehaus, and S. Irle, "The Fragment Molecular Orbital Method Based on Long-Range Corrected Density-Functional Tight-Binding," *Journal of Chemical Theory and Computation* 15, no. 5 (2019): 3008–3020.

25. C. Riplinger and F. Neese, "An Efficient and Near Linear Scaling Pair Natural Orbital Based Local Coupled Cluster Method," *Journal of Chemical Physics* 138, no. 3 (2013): 034106, https://doi.org/10.1063/1.4773581.

26. Y. Guo, C. Riplinger, U. Becker, et al., "Communication: An Improved Linear Scaling Perturbative Triples Correction for the Domain Based Local Pair-Natural Orbital Based Singles and Doubles Coupled Cluster Method [DLPNO-CCSD(T)]," *Journal of Chemical Physics* 148, no. 1 (2018): 011101, https://doi.org/10.1063/1.5011798.

27. A. V. Marenich, C. J. Cramer, and D. G. Truhlar, "Universal Solvation Model Based on Solute Electron Density and on a Continuum Model of the Solvent Defined by the Bulk Dielectric Constant and Atomic Surface Tensions," *Journal of Physical Chemistry B* 113, no. 18 (2009): 6378–6396.

28. A. Klamt and G. Schüürmann, "COSMO: A New Approach to Dielectric Screening in Solvents With Explicit Expressions for the Screening Energy and Its Gradient," *Journal of the Chemical Society, Perkin Transactions 2* 5 (1993): 799–805.

29. M. Antonietti, D. Kuang, B. Smarsly, and Y. Zhou, "Ionic Liquids for the Convenient Synthesis of Functional Nanoparticles and Other Inorganic Nanostructures," *Angewandte Chemie International Edition* 43, no. 38 (2004): 4988–4992.

30. M. T. d. N. Varella, L. Stojanović, V. Q. Vuong, S. Irle, T. A. Niehaus, and M. Barbatti, "How the Size and Density of Charge-Transfer Excitons Depend on Heterojunction's Architecture," *Journal of Physical Chemistry C* 125, no. 10 (2021): 5458–5474, https://doi.org/10.1021/acs.jpcc.0c10762.

31. M. Pan, N. Cao, W. Lin, et al., "Reversible CO_2 Capture by Conjugated Ionic Liquids Through Dynamic Covalent Carbon–Oxygen Bonds," *ChemSusChem* 9, no. 17 (2016): 2351–2357.

32. F. Neese, "WIREs Computational Molecular Science," *WIREs Computational Molecular Science* 12, no. 5 (2022): e1606, https://doi.org/10.1002/wcms.1606.

33. F. Neese, F. Wennmohs, U. Becker, and C. Riplinger, "The ORCA Quantum Chemistry Program Package," *Journal of Chemical Physics* 152, no. 22 (2020): 224108, https://doi.org/10.1063/5.0004608.

34. T. H. Dunning, Jr., "Gaussian Basis Sets for Use in Correlated Molecular Calculations. I. The Atoms Boron Through Neon and Hydrogen," *Journal of Chemical Physics* 90, no. 2 (1989): 1007–1023.

35. D. E. Woon and T. H. Dunning, Jr., "Gaussian Basis Sets for Use in Correlated Molecular Calculations. III. The Atoms Aluminum Through Argon," *Journal of Chemical Physics* 98, no. 2 (1993): 1358–1371, https://doi.org/10.1063/1.464303.

36. D. Datta, S. Kossmann, and F. Neese, "Analytic Energy Derivatives for the Calculation of the First-Order Molecular Properties Using the Domain-Based Local Pair-Natural Orbital Coupled-Cluster Theory," *Journal of Chemical Physics* 145, no. 11 (2016): 114101, https://doi.org/10.1063/1.4962369.

37. F. Weigend, A. Köhn, and C. Hättig, "Efficient Use of the Correlation Consistent Basis Sets in Resolution of the Identity MP2 Calculations," *Journal of Chemical Physics* 116, no. 8 (2002): 3175–3183.

38. C. Hättig, "Optimization of Auxiliary Basis Sets for RI-MP2 and RI-CC2 Calculations: Core–Valence and Quintuple-ζ Basis Sets for H to Ar and QZVPP Basis Sets for Li to Kr," *Physical Chemistry Chemical Physics* 7, no. 1 (2005): 59–66.

39. A. D. Becke, "A New Mixing of Hartree–Fock and Local Density-Functional Theories," *Journal of Chemical Physics* 98, no. 2 (1993): 1372–1377.

40. A. D. Becke, "Density-Functional Thermochemistry. III. The Role of Exact Exchange," *Journal of Chemical Physics* 98, no. 7 (1993): 5648–5652.

41. O. A. Vydrov, J. Heyd, A. V. Krukau, and G. E. Scuseria, "Importance of Short-Range Versus Long-Range Hartree-Fock Exchange for the Performance of Hybrid Density Functionals," *Journal of Chemical Physics* 125, no. 7 (2006): 074106, https://doi.org/10.1063/1.2244560.

42. O. A. Vydrov and G. E. Scuseria, "Assessment of a Long-Range Corrected Hybrid Functional," *Journal of Chemical Physics* 125, no. 23 (2006): 234109, https://doi.org/10.1063/1.2409292.

43. T. Clark, J. Chandrasekhar, G. W. Spitznagel, and P. V. R. Schleyer, "Efficient Diffuse Function-Augmented Basis Sets for Anion Calculations. III. The 3-21 + G Basis Set for First-Row Elements, Li–F," *Journal of Computational Chemistry* 4, no. 3 (1983): 294–301.

44. M. M. Francl, W. J. Pietro, W. J. Hehre, et al., "Self-Consistent Molecular Orbital Methods. XXIII. A Polarization-Type Basis Set for Second-Row Elements," *Journal of Chemical Physics* 77, no. 7 (1982): 3654–3665.

45. R. Krishnan, J. S. Binkley, R. Seeger, and J. A. Pople, "Self-Consistent Molecular Orbital Methods. XX. A Basis Set for Correlated Wave Functions," *Journal of Chemical Physics* 72, no. 1 (2008): 650–654.

46. A. D. McLean and G. S. Chandler, "Contracted Gaussian Basis Sets for Molecular Calculations. I. Second Row Atoms, $Z = 11–18$," *Journal of Chemical Physics* 72, no. 10 (2008): 5639–5648.

47. G. W. Spitznagel, T. Clark, P. von Ragué Schleyer, and W. J. Hehre, "An Evaluation of the Performance of Diffuse Function-Augmented Basis Sets for Second Row Elements, Na-cl," *Journal of Computational Chemistry* 8, no. 8 (1987): 1109–1116.

48. I. Lage-Estebanez, L. del Olmo, R. López, and J. M. García de la Vega, "The Role of Errors Related to DFT Methods in Calculations Involving Ion Pairs of Ionic Liquids," *Journal of Computational Chemistry* 38, no. 8 (2017): 530–540, https://doi.org/10.1002/jcc.24707.

49. M. D. Hanwell, D. E. Curtis, D. C. Lonie, T. Vandermeersch, E. Zurek, and G. R. Hutchison, "Avogadro: An Advanced Semantic Chemical Editor, Visualization, and Analysis Platform," *Journal of Cheminformatics* 4, no. 1 (2012): 17.

50. B. Hourahine, B. Aradi, V. Blum, et al., "DFTB+, a Software Package for Efficient Approximate Density Functional Theory Based Atomistic Simulations," *Journal of Chemical Physics* 152, no. 12 (2020): 124101, https://doi.org/10.1063/1.5143190.

51. S. Grimme, J. Antony, S. Ehrlich, and H. Krieg, "A Consistent and Accurate Ab Initio Parametrization of Density Functional Dispersion Correction (DFT-D) for the 94 Elements H-Pu," *Journal of Chemical Physics* 132, no. 15 (2010): 154104, https://doi.org/10.1063/1.3382344.

52. M. Gaus, Q. Cui, and M. Elstner, "Density Functional Tight Binding: Application to Organic and Biological Molecules," *WIREs Computational Molecular Science* 4, no. 1 (2014): 49–61.

53. J. G. Brandenburg and S. Grimme, "Accurate Modeling of Organic Molecular Crystals by Dispersion-Corrected Density Functional Tight Binding (DFTB)," *Journal of Physical Chemistry Letters* 5, no. 11 (2014): 1785–1789.

54. S. Grimme, S. Ehrlich, and L. Goerigk, "Effect of the Damping Function in Dispersion Corrected Density Functional Theory," *Journal of Computational Chemistry* 32, no. 7 (2011): 1456–1465.

55. M. Gaus, A. Goez, and M. Elstner, "Parametrization and Benchmark of DFTB3 for Organic Molecules," *Journal of Chemical Theory and Computation* 9, no. 1 (2013): 338–354.

56. A. V. Onufriev and D. A. Case, "Generalized Born Implicit Solvent Models for Biomolecules," *Annual Review of Biophysics* 48 (2019): 275–296.

57. S. Ehlert, M. Stahn, S. Spicher, and S. Grimme, "Robust and Efficient Implicit Solvation Model for Fast Semiempirical Methods," *Journal of Chemical Theory and Computation* 17, no. 7 (2021): 4250–4261.

58. E. Miliordos and S. S. Xantheas, "On the Validity of the Basis Set Superposition Error and Complete Basis Set Limit Extrapolations for the Binding Energy of the Formic Acid Dimer," *Journal of Chemical Physics* 142, no. 23 (2015): 094311, https://doi.org/10.1063/1.4913766.

59. J. P. Heindel, Q. Yu, J. M. Bowman, and S. S. Xantheas, "Benchmark Electronic Structure Calculations for $H_3O + (H_2O)n$, $n = 0–5$, Clusters and Tests of an Existing 1,2,3-Body Potential Energy Surface With a New 4-Body Correction," *Journal of Chemical Theory and Computation* 14, no. 9 (2018): 4553–4566.

60. J. Rigby and E. I. Izgorodina, "Assessment of Atomic Partial Charge Schemes for Polarisation and Charge Transfer Effects in Ionic Liquids," *Physical Chemistry Chemical Physics* 15, no. 5 (2013): 1632–1646.

Supporting Information

Additional supporting information can be found online in the Supporting Information section.